

UCLA

UCLA Previously Published Works

Title

Noninvasive optical and nuclear imaging of Staphylococcus-specific infection with a human monoclonal antibody-based probe

Permalink

<https://escholarship.org/uc/item/7nv0d534>

Journal

Virulence, 9(1)

ISSN

2150-5594

Authors

Pastrana, Francisco Romero

Thompson, John M

Heuker, Marjolein

et al.

Publication Date

2018-12-31

DOI

10.1080/21505594.2017.1403004

Copyright Information

This work is made available under the terms of a Creative Commons Attribution-NonCommercial-NoDerivatives License, available at

<https://creativecommons.org/licenses/by-nc-nd/4.0/>

Peer reviewed

RESEARCH PAPER



Noninvasive optical and nuclear imaging of *Staphylococcus*-specific infection with a human monoclonal antibody-based probe

Francisco Romero Pastrana^{a,#}, John M. Thompson^{b,#}, Marjolein Heuker^a, Hedzer Hoekstra^a, Carly A. Dillen^c, Roger V. Ortines^c, Alyssa G. Ashbaugh^c, Julie E. Pickett^d, Matthijs D. Linssen^{e,f}, Nicholas M. Bernthal^g, Kevin P. Francis^{g,h,i}, Girbe Buist^a, Marleen van Oosten^a, Gooitzen M. van Damⁱ, Daniel L. J. Thorek^{d,j}, Lloyd S. Miller^{b,c,k,#}, and Jan Maarten van Dijk^{a,#}

^aDepartment of Medical Microbiology, University of Groningen, University Medical Center Groningen, Hanzeplein 1, Groningen, RB, The Netherlands; ^bDepartment of Orthopaedic Surgery, Johns Hopkins University School of Medicine, Baltimore, MD, USA; ^cDepartment of Dermatology, Johns Hopkins University School of Medicine, Baltimore, MD, USA; ^dDivision of Nuclear Medicine and Molecular Imaging, Department of Radiology and Radiological Science, Johns Hopkins University School of Medicine, Baltimore, MD, USA; ^eDepartment of Gastroenterology and Hepatology, University of Groningen, University Medical Center Groningen, Hanzeplein 1, Groningen, RB, The Netherlands; ^fDepartment of clinical Pharmacy and Pharmacology, University of Groningen, University Medical Center Groningen, Hanzeplein 1, Groningen, RB, The Netherlands; ^gDepartment of Orthopaedic Surgery, David Geffen School of Medicine at the University of California, Los Angeles Medical Center, Santa Monica, CA, USA; ^hPerkinElmer, Alameda, California, CA, USA; ⁱDepartment of Surgery, Nuclear Medicine and Molecular Imaging and Intensive Care, University of Groningen, University Medical Center Groningen, Hanzeplein 1, Groningen, RB, The Netherlands; ^jDepartment of Oncology, Sidney Kimmel Comprehensive Cancer Center, Johns Hopkins University School of Medicine, Baltimore, MD, USA; ^kDivision of Infectious Disease, Department of Medicine, Johns Hopkins University School of Medicine, Baltimore, MD, USA

ABSTRACT

Staphylococcus aureus infections are a major threat in healthcare, requiring adequate early-stage diagnosis and treatment. This calls for novel diagnostic tools that allow noninvasive in vivo detection of staphylococci. Here we performed a preclinical study to investigate a novel fully-human monoclonal antibody 1D9 that specifically targets the immunodominant staphylococcal antigen A (IsaA). We show that 1D9 binds invariantly to *S. aureus* cells and may further target other staphylococcal species. Importantly, using a human post-mortem implant model and an in vivo murine skin infection model, preclinical feasibility was demonstrated for 1D9 labeled with the near-infrared fluorophore IRDye800CW to be applied for direct optical imaging of in vivo *S. aureus* infections. Additionally, ⁸⁹Zirconium-labeled 1D9 could be used for positron emission tomography imaging of an in vivo *S. aureus* high infection model. Our findings pave the way towards clinical implementation of targeted imaging of staphylococcal infections using the human monoclonal antibody 1D9.

ARTICLE HISTORY

Received 26 April 2017
Revised 4 October 2017
Accepted 2 November 2017

KEYWORDS



human monoclonal antibody; immunodominant staphylococcal antigen A; IsaA; PET; ⁸⁹Zr; *Staphylococcus aureus*

Introduction

The rapid and accurate diagnosis of a bacterial infection is important for the initiation of appropriate medical and surgical management. Traditional diagnostic approaches involve microbiological techniques, histologic staining and, more recently, molecular techniques. However, these approaches require sampling of infected tissues, which involves invasive procedures that add cost and potential morbidity, as uninfected tissue or implants are exposed to bacteria from the skin microbiota and surgical environment. Also, culture-based diagnostic approaches are

inherently fraught with issues of sampling error and contamination. Since current diagnostic tests often take days to deliver results, antibiotic therapy is frequently started empirically, and this can lead to inadequate or incorrect treatment, contributing to worse clinical outcomes. The problems with current diagnosis of infection are particularly relevant for infections caused by *Staphylococcus aureus*, which is responsible for the majority of skin and soft tissue infections, as well as invasive and life-threatening infections, such as cellulitis, pneumonia, osteomyelitis and bacteremia.¹ *S. aureus* is also a common cause of

CONTACT Jan Maarten van Dijk  j.m.van.dijk01@umcg.nl

 Supplemental data for this article can be accessed on the  publisher's website.

[#]These authors contributed equally to this work.

© 2018 The Author(s). Published by Informa UK Limited, trading as Taylor & Francis Group

This is an Open Access article distributed under the terms of the Creative Commons Attribution-NonCommercial-NoDerivatives License (<http://creativecommons.org/licenses/by-nc-nd/4.0/>), which permits non-commercial re-use, distribution, and reproduction in any medium, provided the original work is properly cited, and is not altered, transformed, or built upon in any way.

medical device and implant-related infections, which are exceedingly difficult to treat because the bacteria form biofilms on the foreign materials that inhibit the efficacy of antibiotics. Rapid detection and treatment prior to the seeding of implants and establishment of biofilm is essential. Moreover, the widespread emergence of methicillin-resistant *S. aureus* (MRSA) strains, which are resistant to multiple antibiotics,^{2,3} is causing substantial delays in starting adequate antibiotics coverage. This highlights the need for faster, more sensitive and noninvasive diagnostic alternatives than are currently available.

Current noninvasive imaging modalities used to localize infection foci include computed tomography, positron emission tomography (PET) with fluorine-18-fluorodeoxyglucose, and magnetic resonance imaging. However, these approaches cannot accurately differentiate between infected tissue and sterile inflammation. Therefore, there have been intense efforts to develop more targeted imaging techniques by using bacteria-specific tracers, which typically consist of a targeting moiety with affinity for bacteria conjugated to an imaging agent for optical, optoacoustic or PET imaging.^{4,5} Promising tracers have combined antibodies, antibiotics, antimicrobial peptides, metabolizable compounds or particular ligands with attached fluorophores or radioisotopes.^{4,6–8} However, the vast majority of these tracers has been designed to detect infections caused by a broad spectrum of bacterial species, while relatively few studies have explored species-specific tracers.^{9–12}

We have recently provided proof-of-principle for the use of antibiotic-based targeting probes labeled with near-infrared (NIR) fluorophores for optical and optoacoustic imaging, demonstrating preclinical detection of *S. aureus* infections.^{5,13} However, antibiotics generally lack the ability to identify specific bacterial species as most have broad affinity, binding indiscriminately to Gram-positive and/or Gram-negative bacteria. Species-specific tracers offer the potential to not only identify the presence of an infection, but to define the causative organism, thereby providing an actionable diagnosis that could guide targeted antibiotic therapy. This is especially relevant to invasive *S. aureus* infections, such as necrotizing pneumonia and endocarditis, or difficult-to-treat biofilm-related infections. Such targets for staphylococcal-specific imaging might include proteins exposed on the bacterial cell surface.^{14–16} A well-conserved surface protein of *S. aureus* is the immunodominant staphylococcal antigen A (IsaA).^{17–21} In a previous study, we developed a fully human monoclonal antibody (humAb) against IsaA, which was partially protective against *S. aureus* infections in mouse models.²² In the present preclinical study we investigated the target specificity of this anti-

IsaA humAb, named 1D9, using an extensive panel of different staphylococcal isolates, and explored the feasibility of using 1D9 conjugated with the NIR fluorophore IRDye 800CW or the PET tracer ⁸⁹Zr as an *S. aureus*-specific tracer in a human post-mortem infection model and in in vivo mouse models of *S. aureus* infection.

Results and Discussion

High target sensitivity of humAb 1D9 for *S. aureus*

A key feature of an effective targeting moiety for the specific detection of an infecting pathogen is the ability to bind to the vast majority of different clinically related isolates. A BLASTP analysis indicated that the *isaA* gene was present in all of the 1912 different *S. aureus* isolates for which sequences are available, with respective IsaA proteins showing at least 98% amino acid sequence identity. In addition, the *isaA* gene was found to be conserved in several other staphylococcal species. When *S. aureus* isolates were excluded from the BLASTP results, significant hits with at least 60% identity at the amino acid sequence level were obtained for *S. epidermidis* (145), *S. argenteus* (6), *S. warneri* (5), *S. schweitzeri* (3), *S. simiae* (2), and *S. haemolyticus* (1). Additional identified staphylococcal species with lower identity scores (<60%) for IsaA included *S. caprae*, *S. delphini*, *S. hominis*, *S. intermedius*, *S. lugdunensis*, *S. microti*, *S. pasteurii*, *S. pseudintermedius*, *S. schleiferi*, *S. schweitzeri*, and *S. simulans*. These findings suggest that the respective species produce IsaA proteins that may be detectable with 1D9. To confirm these results, Western blotting analysis was performed with 1D9. 1D9 detected IsaA production in well-described MRSA strains, including USA300, Mu50, MW2, N315, COL and MRSA252 (Fig. 1A). IsaA production was also detected with 1D9 in the laboratory strain NCTC8325-4 as well as additional clinical *S. aureus* isolates from the University Medical Center Groningen (isolates A–Y; Fig. 1A, B). Of note, IsaA was always detected in the cell fraction and in most (but not all) growth medium fractions. To control for any off-target binding of 1D9 to different *S. aureus* proteins known to bind to the Fc portion of human IgG1 (*i.e.*, protein A [Spa] and Sbi),¹⁵ cell and medium fractions from *S. aureus* Newman wild-type and Δspa or $\Delta spa \Delta sbi$ mutant derivatives were tested for 1D9 binding. 1D9 bound to IsaA irrespective of the presence of Spa and Sbi (Fig. 1C). From a test panel of other *Staphylococcus* species, IsaA-specific signals were observed for two out of four *S. epidermidis* isolates, two tested *S. hominis* isolates, as well as an isolate of *S. pettenkoferi* and *S. caprae* (Fig. 1C). IsaA expression was not detected in *S. lugdunensis*, *S. haemolyticus*, *S. capitis*, *S. warneri* and *S.*

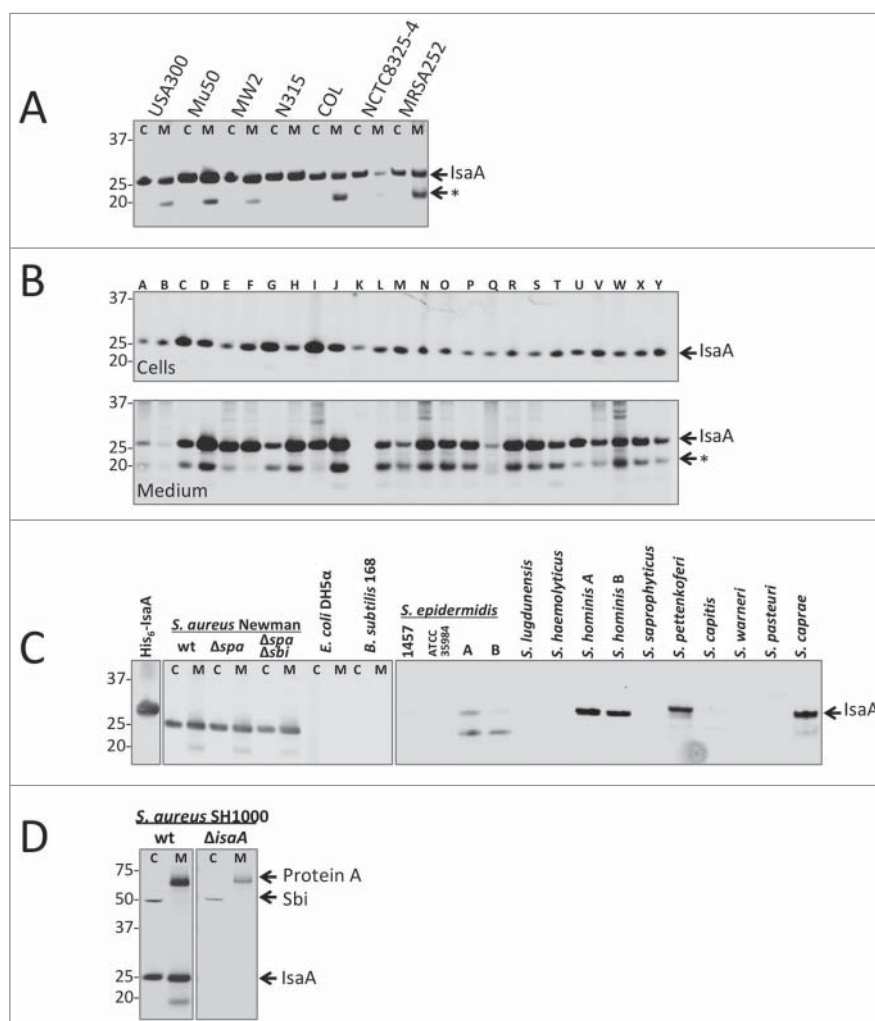


Figure 1. IsaA expression in *S. aureus* and other staphylococcal species. Detection of IsaA production in (A) sequenced *S. aureus* strains and (B) 25 clinical *S. aureus* isolates (A – Y) by Western blotting and immunodetection with 1D9-800CW. (C) Western blotting analysis for IsaA detection in *spa* and *spa sbi* mutants of *S. aureus* Newman, *E. coli* DH5 α , *B. subtilis* 168 and several different staphylococcal species. Left panel, immunodetection of IsaA with unlabeled 1D9 and a secondary IRDye800CW-labeled goat anti-human antibody; right panel immunodetection with 1D9-800CW. Purified His₆-IsaA was used as a control. (D) Western blotting analysis to verify the absence of IsaA production in *S. aureus* MS001 ($\Delta isaA$) using 1D9-800CW for immunodetection. C, cell fraction; M, growth medium fraction. The positions of molecular weight markers are indicated on the left, and the positions of IsaA, an IsaA degradation product (*), Protein A and Sbi are indicated on the right.

pasteuri, nor in *Bacillus subtilis* 168 or *Escherichia coli* DH5 α controls (Fig. 1C). As expected, no IsaA signal was detectable in the cell and growth medium fractions of an *isaA* deletion mutant (Fig. 1D). Taken together, these findings imply that 1D9 can be used to specifically detect cells of the vast majority of *S. aureus* isolates plus a number of additional clinically-applicable staphylococcal species.

Imaging of 1D9-800CW labeled bacteria in a human post-mortem implant model

The ability of 1D9 to provide in vivo detection of *S. aureus* was first assessed in a post-mortem model where

Whatman filter paper soaked with bacteria was implanted subdermally on the tibia of a human cadaver with subsequent skin closure.¹³ To enable NIR imaging, 1D9 was conjugated to the fluorophore IRDye 800CW, and the resulting 1D9-800CW complex was added to wild-type *S. aureus* bacteria. To assess the contribution of IgG-binding proteins Spa and Sbi to the signal, *S. aureus* mutant strains lacking both *spa* and *sbi* ($\Delta spa \Delta sbi$) were also probed with 1D9-800CW. We additionally included a *S. aureus* mutant strain lacking *isaA* ($\Delta isaA$) and *S. epidermidis* 1457 that are both negative for binding 1D9 (Fig. 1). All cells incubated with 1D9-800CW were thoroughly washed in phosphate-buffered saline (PBS) and spotted in equal amounts (2.5×10^8

CFU) onto a Whatman filter paper. NIR images of the filter paper were recorded prior to and during ~ 8 mm subdermal implantation in the post-mortem model. As shown in Fig. 2, the strongest NIR signal was observed for wild-type *S. aureus*. A slightly lower signal was observed for the $\Delta spa \Delta sbi$ double mutant, indicating that 1D9-800CW binding to IgG-binding proteins contributed minimally to the observed signal. In comparison, the signal observed for the *isaA* mutant cells was significantly lower, confirming that Spa and Sbi bind

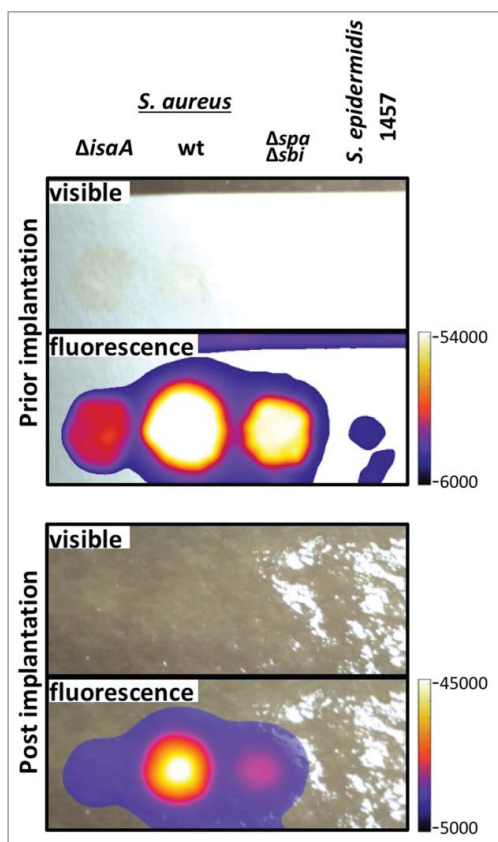


Figure 2. Human post-mortem implant model. For near-infrared fluorescent imaging of staphylococcal cells in a human post-mortem model, overnight grown cultures of *S. aureus* MS001 ($\Delta isaA$), *S. aureus* SH1000 (wt), *S. aureus* Newman $\Delta spa \Delta sbi$ ($\Delta spa \Delta sbi$) and *S. epidermidis* 1457 in TSB (5×10^8 , CFU) were collected, washed twice with PBS, resuspended in $100 \mu\text{l}$ of PBS, and incubated with $5 \mu\text{g}$ of 1D9-800CW. Upon 20 min incubation at room temperature, cells were washed twice with PBS and resuspended in $100 \mu\text{l}$ of PBS. Of this suspension with fluorescently labeled cells, $50 \mu\text{l}$ aliquots were spotted on filter paper strips (Whatman), and placed inside sealed plastic wrapping. Visible light and fluorescence images were recorded prior to and during surgical implantation onto the distal tibia of a human post-mortem leg. Fluorescence imaging was performed using an intraoperative clinical multi-spectral fluorescence eXplorer Air camera (SurgVision BV). Fluorescence signals were collected 0.5 sec (before implantation) and 0.2 sec (during implantation) with low binning and excitation/emission wavelengths of 740/845 nm.

relatively minor amounts of 1D9-800CW compared to *IsaA*. Minimal signal was detectable for *S. epidermidis* 1457, which is consistent with the Western blotting data in Fig. 1C. Importantly, the signal from the 1D9-800CW bound to wild-type cells was clearly detectable upon implantation and suturing of the skin, providing proof-of-principle that 1D9 can be used for detection of subdermal *S. aureus* infections in humans.

Noninvasive in vivo fluorescent imaging of *S. aureus* infection with 1D9-800CW

To validate the potential use of 1D9-800CW for specific in vivo imaging of *S. aureus* infections, a murine skin infection and inflammation model was used. In a first group of mice, opposite flanks of each mouse were inoculated intradermally with a bioluminescent wild-type *S. aureus* SH1000 strain (wt) and the isogenic *isaA* mutant MS001 ($\Delta isaA$). In parallel, a group of control mice were inoculated in opposite flanks with bioluminescent *E. coli* Xen14 (*Ec*) and lipopolysaccharide (LPS) to evaluate any off-target accumulation at a site of either an infection caused by a bacterium that does not express *IsaA* or sterile inflammation. One day post-inoculation, 2.5 mg/kg 1D9-800CW was administered intravenously. Fluorescence and bioluminescence were recorded one day prior to inoculation (t_{-2}), one hour after inoculation (t_{-1}), immediately before 1D9-800CW administration (t_0), at 2/4/8 h after administration, and daily thereafter (t_{1-7}) (Fig. 3). From day 1 onwards, significantly higher fluorescent signal was localized in the flanks of mice infected with the wt *S. aureus* strain compared to the $\Delta isaA$ mutant ($P < 0.01$), *E. coli* Xen14 ($P < 0.0001$), or LPS ($P < 0.001$) (Fig. 3A, B). The significant difference observed for the wt and $\Delta isaA$ *S. aureus* strains implies that, similar to the post-mortem model (Fig. 2), 1D9-800CW binds to the *IsaA* target rather than the IgG Fc-binding proteins Spa and Sbi. Importantly, the stronger fluorescence signals observed for the *S. aureus* isolates compared to the fluorescence signals elicited by *E. coli* Xen14 or LPS show that 1D9-800CW is specific for *S. aureus*, and that *S. aureus* infection overall can be distinguished from other causative infections or LPS-induced sterile inflammation. However, an early peak of fluorescence observed for mice inoculated with LPS indicates that 1D9-800CW does accumulate at early time points at the site of sterile inflammation (Fig. 3B). This is possibly due to the Enhanced Permeability and Retention (EPR) effect resulting from inflammation, or a higher local density of neutrophils and hence Fc-receptor binding of the 1D9 humAb. This effect was not

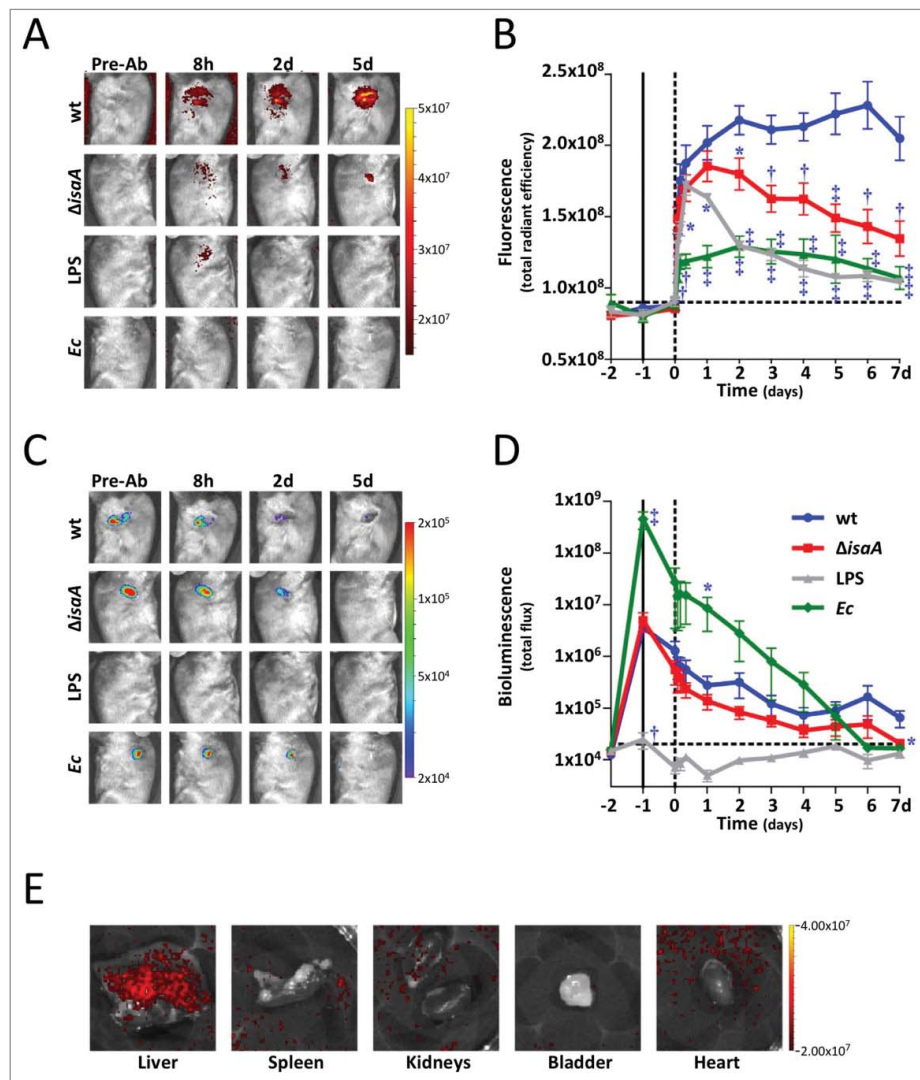


Figure 3. In vivo IsA-specific optical imaging of *S. aureus* infection with 1D9-800CW. Six to eight weeks old C57BL/6 female mice were shaved on the flanks and back, and mid-logarithmic growth phase *S. aureus* SH1000 *lux* (wt) and $\Delta isaA$ *S. aureus* MS001 *lux* (5×10^7 CFUs in $100 \mu\text{l}$ of sterile saline) were each injected intradermally into opposite flanks of each mouse ($n = 7$ performed over 3 independent experiments). In a second group of mice, *E. coli* Xen14 (*Ec*; 5×10^7 CFUs in $100 \mu\text{l}$ of sterile saline) and lipopolysaccharide (LPS; 1 mg/kg in $100 \mu\text{l}$ of sterile saline) were injected intradermal into opposite flanks of each mouse ($n = 4$ performed over 1 experiment). Inoculations were performed on t_{-1} . Control images were recorded 1 day prior to inoculation (t_0) or 1 h after LPS injection, 1D9-800CW (2.5 mg/kg in $100 \mu\text{l}$ sterile saline warmed to 37°C) was injected retro-orbitally and images were subsequently recorded at different time points as indicated. The fluorescent (total radiant efficiency [photons/s]/[mW/cm²]) and bioluminescent signals (total radiance [photons/s]) were measured with a 1.2×1.2 cm region of interest (ROI) centered over the site of skin infection/inflammation. (A) NIR fluorescence images of representative mice were collected at 0.5 sec with medium binning and excitation/emission wavelengths of 740/845 nm. (B) Mean total radiant efficiency (photons/s)/(mW/cm²) \pm s.e.m. of the in vivo fluorescent signals. (C) Bioluminescence images of representative mice were collected for 60 sec with medium binning. (D) Mean total flux (photons/sec) \pm s.e.m. (logarithmic scale) of in vivo bioluminescent signals. (E) Representative NIR fluorescence images of different organs collected on day 2 for assessment of 1D9-800CW accumulation. In panels B and D, variations are indicated with error bars and statistically significant differences with different symbols for each curve (* = $P < 0.05$; † = $P < 0.01$; ‡ = $P < 0.001$).

observed when the mice were inoculated with *E. coli*, suggesting that LPS induced a stronger inflammatory response than *E. coli*. Importantly, the signal became more specific from 2 days onwards. Further, the bioluminescence signals of the three bacterial strains were not significantly different (Fig. 3C, D), showing that differences in fluorescence signal were due to

specificity for *S. aureus* rather than the bacterial inoculum. Harvested organs on day 2 showed that fluorescence was mostly concentrated in the liver, with no appreciable signals in the spleen, kidneys, bladder or heart (Fig. 3E), which is consistent with the known clearance of antibodies by the liver. Of note, all bioluminescence signals at sites of infection decreased over

time, which could relate to reduced growth, loss of the pLux plasmid that was used to make the bacteria bioluminescent and/or bacterial clearance. For example, we have previously shown that luminescence of the bacteria is significantly reduced once they reach the stationary phase of growth.¹³ In contrast, the 1D9 antibody will bind to IsaA irrespective of whether the bacteria are dead or alive. This would explain why a stable signal for 1D9-800CW was observed at time points post infection where the bioluminescence signal had disappeared. In addition, culturing of infected mouse tissue showed that some *S. aureus* CFU had lost the pLux plasmid (data not shown). Altogether, it seems that the loss of luminescence was probably both related to reduced growth and loss of the pLux plasmid. Yet, it cannot be excluded that a slight decrease in bacterial numbers by immune clearance contributed to the loss of the luminescence signal at the site of infection.

Since the above set of experiments involved two groups of mice inoculated in parallel, an independent

experiment was performed where opposite flanks of the same mice were inoculated intradermally with a bioluminescent community-acquired MRSA strain (SAP231) and *E. coli* Xen14. In both of these bacterial strains, the *lux* genes for bioluminescence are stably integrated into the chromosome and are thus present in all progeny. Similar to the prior experiment, the fluorescent signals of 1D9-800CW were higher at the site of the *S. aureus* infection compared with the *E. coli* infection (Fig. 4A, B), showing the specificity of 1D9-800CW for *S. aureus*. Likewise, the bioluminescent signals of the infecting bacteria both decreased over time (Fig. 4C, D), suggesting reduced bacterial growth and/or clearance. A noteworthy observation was that the 1D9-800CW signal relating to *S. aureus* infection was highly stable over 7 days, which is in line with the known half-life of IgG1 humAbs of 6–8 days in mice. Since the half-life of IgG1 humAbs in humans is ~3 weeks, our findings imply that this particular probe can be used over several days upon administration, which is a clear advantage for potential clinical applications.

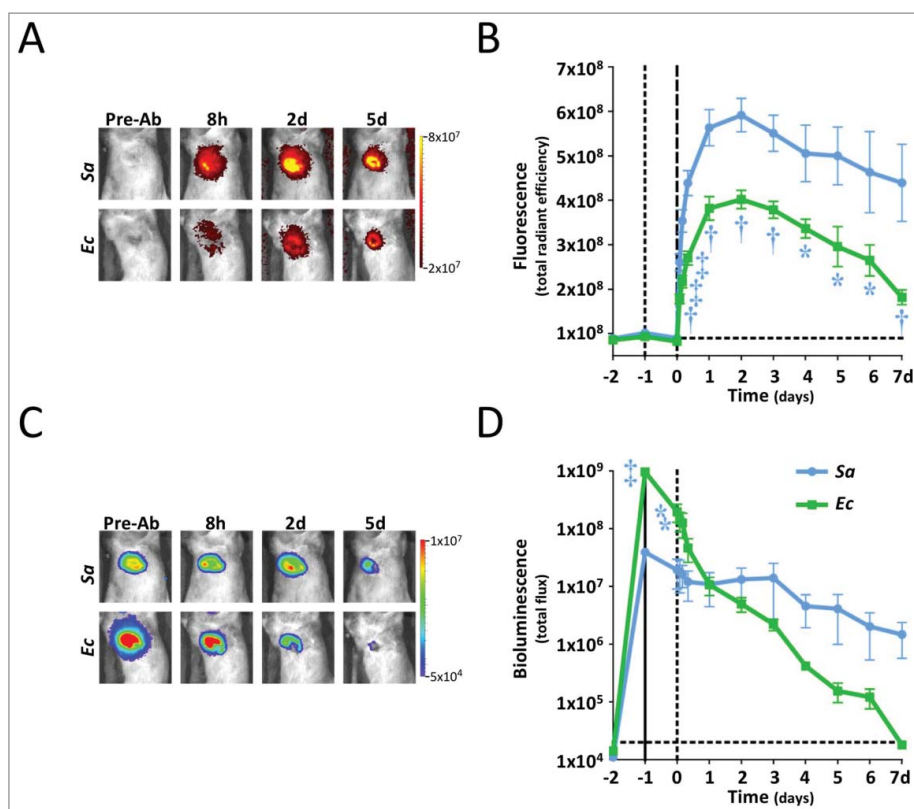


Figure 4. Distinction of *S. aureus* and *E. coli* infection by optical imaging with 1D9-800CW. Mice were inoculated intradermally in opposite flanks with bioluminescent *S. aureus* SAP231 (SAP) and *E. coli* Xen14 (Ec) as described for Fig. 3. Images were recorded at different time points pre and post intravenous administration of 2.5 mg/kg 1D9-800CW. (A) NIR fluorescence images of representative mice were collected with excitation/emission wavelengths of 740/845 nm. (B) Mean total radiant efficiency (photons/s)/(mW/cm²) \pm s.e.m. of the *in vivo* fluorescent signals. (C) Bioluminescence images of representative mice. (D) Mean total flux (photons/sec) \pm s.e.m. (logarithmic scale) of *in vivo* bioluminescent signals. In panels B and D, variations are indicated with error bars and statistically significant differences with different symbols for each curve (* = P < 0.05; † = P < 0.01; ‡ = P < 0.001).

Previously, we have shown that the antibiotic vancomycin labeled with IRDye800CW (*i.e.*, vanco-800CW) also allows for highly specific noninvasive *in vivo* detection of infecting staphylococci. However, vanco-800CW detects a broad spectrum of Gram-positive bacteria.¹³ In contrast, a positive signal obtained with 1D9-800CW is diagnostic for potentially virulent staphylococci.

Noninvasive *in vivo* PET imaging of *S. aureus* infection with ⁸⁹Zr-1D9

NIR fluorescence imaging of infection is appealing due to its speed, noninvasiveness and high resolution. In addition, it does not involve the use of radioactive isotopes, which makes it less expensive and more flexible than PET or single-photon emission computed tomography imaging, as well as circumventing the burden of ionizing radiation.⁴ Despite these advantages, one major drawback of NIR fluorescent imaging is the limited signal penetration through tissue, which is about 1 cm due to light absorption and scatter.⁴ For these reasons, we also explored the possibility of applying 1D9 to whole-body PET imaging to see if this modality would allow the high-sensitivity delineation of deeper-seated infections with clinical significance. Thus, 1D9 was labeled with ⁸⁹Zr, which has a half-life of 78.4 h. Similar to the experiments shown in Fig. 3A, B, opposite flanks of each mouse were inoculated with wt *S. aureus* SH1000 and the isogenic *isaA* mutant MS001 ($\Delta isaA$). At 1 day *post-infection*, 0.7 mg/kg of ⁸⁹Zr-1D9 was administered and PET images were recorded on days 3, 5, and 7. As shown in Fig. 5A, B, ⁸⁹Zr-1D9 revealed a specific accumulation at the site of infection, with a significantly higher intensity for the

infection caused by wild-type *S. aureus* compared to the infection by *IsaA*-deficient *S. aureus*. Statistically significant differences between the specific and control infections were detected for 3 days. However, due to the limited half-life of ⁸⁹Zr, imaging was only possible for up to 7 days. Of note, Fig. 5A shows a strong signal in the body, which is consistent with the data presented in Fig. 3E where the accumulation of 1D9-800CW in the liver is shown. For potential clinical applications in the future, the known clearance of antibodies by the liver may thus represent a challenge if one wishes to detect specific signals of endocarditis or other infections near high-uptake organs, such as the liver. However, this is likely to represent less of a problem, if any, for the imaging of infections at body sites distant from the liver.

Future perspectives

Here we present the humAb 1D9 as a highly specific probe for both fluorescence and PET imaging of staphylococcal infections. The high specificity of 1D9 is demonstrated by longitudinal measurements in mouse infection models with extensive controls, in particular recombinant *IsaA*-deficient *S. aureus*, the Gram-negative bacterium *E. coli* and purified LPS. Thus, off-target accumulation of 1D9 at sites of inflammation and infection, *e.g.* due to increased blood flow and vascular permeability, may be ruled out. We consider it important that 1D9 is compatible with PET imaging modalities, because this may permit a faster introduction into the clinic as PET facilities are widely available in hospitals around the globe. Further, our experiments suggest the feasibility of 1D9 applications in optoacoustic imaging,

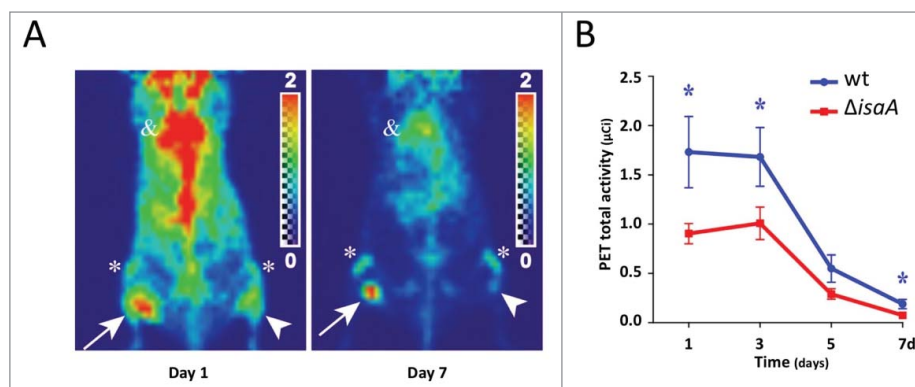


Figure 5. *In vivo* *IsaA*-specific PET imaging of *S. aureus* infection with ⁸⁹Zr-1D9. Mice were inoculated intradermally in opposite flanks with either *S. aureus* SH1000 (wt) or *S. aureus* MS001 ($\Delta isaA$) as described for Fig. 3 (t_0). One day post inoculation (t_0), 0.7 mg/kg ⁸⁹Zr-1D9 was administered intravenously and images were subsequently recorded at different time points as indicated. List-mode data were acquired using a gamma-ray energy window of 350 to 750 keV and a coincidence timing window of 6 ns. PET imaging data were corrected for detector non-uniformity, dead time, random coincidences, and physical decay. For all static images, scan time was between 10 and 20 min. (A) PET images of representative mice [arrows = wt infection; arrowheads = $\Delta isaA$ infection; * = knee joint; & = heart]. (B) PET total activity (μCi) at the site of infection. In panel B, variations are indicated with error bars and statistically significant differences with an asterisk (* = $P < 0.05$).

which has a significantly better tissue penetration (> 8 cm) than light (~ 1 cm).^{4,5} This relates to the fact that agents used in optoacoustic imaging, like indocyanine green, absorb light of a particular wavelength and subsequently undergo thermo-elastic expansion. In turn, this results in the emission of ultrasonic pressure waves, which have much longer wavelengths than light and higher tissue penetration. Importantly, such ultrasonic signals are detectable with special sensors.

The need for rapid noninvasive modalities for infection imaging is highlighted by recent publications on a variety of probes that, together, allow in vivo detection of a broad spectrum of pathogens. For instance, these include probes based on antibiotics,^{4,23} maltodextrin,²⁴ prothrombin,²⁵ oligonucleotides,²⁶ the bacteriophage M13,^{12,27} and concanavalin A.²⁸ In this study, the 1D9 probe was evaluated as a novel and alternative antibody-based probe with the highest target specificity for *S. aureus*. 1D9 labeled with the NIR fluorophore IRDye800CW could be used to continuously monitor infecting bacteria over a period of at least 7 days using in vivo fluorescence imaging. For the imaging of deeper-seated infections, 1D9 labeled with ⁸⁹Zr can be used in conjunction with whole-body PET imaging. We therefore conclude that the humAb 1D9 provides new targeted and specific diagnostic imaging tracers for *S. aureus* infections.

Novel diagnostic technologies, especially next-generation DNA sequencing, are becoming increasingly popular tools for the detection of infections. However, next-generation sequencing is probably best-suited for the detection of superficial infections. For detection of deep-seated infections, the invasive sampling that would be required could be dangerous and is subject to the uncertainties of incorrect sampling and contamination. A potential advantage of using noninvasive imaging in conjunction with a specific monoclonal antibody probe, such as 1D9, is that it may allow the detection of both superficial and deeper seated infections. The latter is particularly the case when the antibody is labeled with a PET tracer, as exemplified in the present study with ⁸⁹Zr-1D9. Given the increasingly common usage of immunoPET imaging, the application of this tool with microgram amounts of antibody could certainly be justifiable in many cases of infection even though the general use of radioactive labels should be restrained. Importantly, not all possible diagnostic applications of the 1D9 antibody will necessarily require radioactive labels. For instance, it is well-conceivable that a fluorescently labeled antibody, like 1D9-800CW, is suitable to guide surgery through intra-operative imaging of infections as is currently explored in cancer imaging.⁴ Further, foci of infection could be detectable by the use of fluorescently labeled antibodies in combination with endoscopy.

Despite the promising results obtained in the present study, the application potential of our humAb 1D9 needs

to be assessed in future ex vivo or in vivo studies. For example, it is currently hard to predict whether the specificity of 1D9 is high enough to discriminate sterile inflammation from infection, especially at early time points after the onset of infection. In addition, it is not yet known how competing circulating antibodies of the host will impact on the efficiency of imaging with labeled 1D9. The latter potential problem can probably be overcome with PET tracers (e.g. ⁸⁹Zr), since part of the appeal of radioactivity is that low antibody binding can still lead to the emission of a sufficiently strong signal to allow accurate measurements. Another important question relates to the need for parallel diagnostics to detect infections caused by pathogens other than *S. aureus*. In this respect, it would be convenient to have a panel of specific monoclonal antibodies targeting major pathogens, like *Pseudomonas*, *Burkholderia*, or *Acinetobacter*. However, as long as such antibodies are not available for infection imaging, approaches based on the 1D9 antibody could be complemented by other tracers that target a broad range of pathogens. For instance, many Gram-positive bacterial pathogens can be detected in vivo with the vancomycin-800CW tracer that we have previously developed.¹³ Infections by Gram-negative bacterial pathogens can potentially be imaged by making use of fluorescently labeled maltodextrin,²⁴ or by radioactively labeled metabolizable compounds, like sorbitol.⁴ On the other hand, it would also be very useful to develop an additional humAb that discriminates between MRSA and methicillin-sensitive *S. aureus*, as is underscored by the increasing incidence of MRSA infections world-wide.

Altogether, we conclude that the present study has achieved preclinical proof-of-principle for the use of the 1D9 monoclonal antibody in the in vivo imaging of infections caused by *S. aureus*. However, before a clinical study on the possible use of our 1D9 antibody can be justified, further animal studies will be needed to answer the questions how effective the 1D9 antibody will be as a diagnostic tool for deep-seated *S. aureus* infections, and for which clinical indications it is best applied.

Materials and Methods

Bacterial strains and growth conditions

Bacterial strains are listed in Supplementary Table 1. Staphylococci were grown at 37°C in Tryptone Soy Broth (TSB). *Escherichia coli* Xen14 was grown at 37°C in Lysogeny Broth (LB; BD Biosciences, Sparks, MD). *Lactococcus lactis* PA1001 was grown at 30°C in M17 broth (Oxoid Limited, Hampshire, UK) with 2% glucose. Media were supplemented with chloramphenicol for plasmid selection (5 µg/ml for pNG4110 and 10 µg/ml for pLux). Plasmid pLux (pbp2-pro) from *S. aureus* ALC2906²⁹ was

introduced by electroporation into *S. aureus* SH1000 and MS001 as reported.^{30,31}

Protein expression, LDS-PAGE and Western blotting

Plasmid pNG4110::*isaA* was constructed by PCR amplification of the *isaA* gene with primers 5'- ataggatccgctgaag-taaacgttgatcaag-3' and 5'- atagcggccgcttagaatcccaagcacctaaaccttg-3', and subsequent cloning in pNG4110.³² Production and expression of His₆-tagged IsaA from plasmid pNG4110::*isaA* was performed as described.³² Bacterial culture supernatants were precipitated with 10% TCA and resuspended in LDS sample buffer (Life Technologies, Grand Island, NY, USA), cells were disrupted with 0.1 μm glass beads (Biospec Products, Bartlesville, USA) in a Precellys 24 homogenizer (Bertin Technologies, France), and liberated proteins were resuspended in Lithium Dodecyl Sulphate (LDS) sample buffer. Samples were analyzed by LDS-PAGE (NuPAGE gels, Life Technologies) and proteins were visualized by protein staining (Simply Blue Safe Staining, Life Technologies) or by blotting onto Protan nitrocellulose transfer paper (Whatman, Germany) and subsequent immunodetection using mouse anti-His-tag antibodies (Life Technologies) or IRDye 800CW-labeled 1D9 antibody. Fluorescent secondary goat anti-human or goat anti-mouse IRDye 800CW antibodies were from LI-COR Biosciences. Antibody binding was visualized using an Odyssey Infrared Imaging System (LI-COR Biosciences, Lincoln, NE, USA).

Antibody production and labeling

The human monoclonal antibody 1D9 was produced as described²² by transient transfection of Expi293F cells (Life Technologies). 1D9 antibodies were isolated by HiTrap Protein A HP column purification (GE Life sciences, Eindhoven, The Netherlands) followed by HiTrap column desalting (GE Life sciences). 1D9 labeling with IRDye 800CW (LI-COR Biosciences) was performed as previously described.³³

Human post-mortem implant model

Near-infrared fluorescent imaging of staphylococcal cells in a human post-mortem model was performed essentially as previously described.¹³

Mouse model and in vivo fluorescence and bioluminescence imaging

Maintenance of C57BL/6 mice and intradermal injection of *S. aureus*, *E. coli* or LPS was performed as previously described.³⁴ In vivo fluorescence and bioluminescence

imaging was performed with an IVIS Lumina III (PerkinElmer, Alameda, CA, USA) essentially as previously described.¹³ Of note, we injected 5×10^7 CFUs of *S. aureus* to provoke intradermal infection, because our previous studies have shown that at least 10^7 CFUs are needed to establish an *S. aureus* infection in our mouse model. Lower numbers of the bacteria will be rapidly cleared by the murine immune system.

Radiolabeling of 1D9 with ⁸⁹Zr

Mild conjugation was used to modify 1D9 with a radio-metal chelate. To antibody in 0.1M HEPES, pH 8.5, three times was added 10 μL of p-SCN-Bn-Deferoxamine (DFO; Macrocyclics, Dallas, TX, USA) in DMSO (233.3 μM) followed by 30–60 min mixing at room temperature to a final DFO:antibody ratio of 7:1. Unreacted DFO was removed using Amicon Ultra 0.5 mL centrifugal filter 50 kDa (EMD Millipore, Billerica, MA, USA). ⁸⁹Zr oxalate was obtained from the Mallinckrodt Institute of Radiology, St. Louis, MO. To ⁸⁹Zr was added an excess of 1 M oxalic acid. 0.1M Na₂CO₃ was slowly added to a pH of 7-7.5. ⁸⁹Zr was added to the DFO-conjugated antibody and mixed at room temperature for 40 min. To chelate unbound ⁸⁹Zr, 50 mM EDTA, pH 5, was added and removed with Amicon Ultra 0.5 mL centrifugal filters using sterile saline. Instant thin layer chromatography (ITLC) was performed using silica impregnated filter paper (Pall Corporation, New York, NY, USA). ITLC was run in 50 mM EDTA, pH 5, and subsequently imaged and quantified using a Phosphor-imager and AutoQuant software (Media Cybernetics, Rockville, MD, USA).

Nuclear and X-ray imaging

The microPET R4 system (Concorde Microsystems Inc., Knoxville, TN, USA) was used to acquire PET scans. For all static images, scan time was between 10 and 20 min. Data were sorted into 3D histograms by Fourier rebinning, and transverse images were reconstructed using a maximum *a priori* algorithm to a 128 × 128 × 63 (0.845 mm × 0.845 mm × 1.2115 mm) matrix. Datasets were analyzed using ASIPro VM microPET software (Siemens Preclinical Solutions, Erlangen, Germany). Volumes of interest were manually defined around areas of bacteria injection and injected activity per gram was calculated. An empirically determined system calibration factor for mice was used to convert voxel count rates to activity concentrations (in μCi per mL of tissue). Figures were generated using Amira (version 5.0; FEI, Hillsboro, OR, USA). Directly after PET scanning, while in the same position, planar images were acquired using the

MX-20-DC12 digital X-ray imaging system (Faxitron Biotronics, Tucson, AZ, USA).

Statistical Analysis

Fluorescence imaging data were analyzed with Prism (GraphPad, La Jolla, CA, USA) and compared using a 1-tailed Student's t-test. Values of $P < 0.05$ were considered significant. All PET imaging data are expressed as mean \pm S.E.M. Data were subjected to the Holm-Sidak method, with $\alpha = 0.05$ and the assumption that all rows are sampled from populations with the same scatter using GraphPad Prism. P-values < 0.05 were considered significant.

Ethics statement

Post-mortem experiments were conducted according to institutional guidelines with prior approval from the scientific review committee of the Skills Center of the University Medical Center Groningen, The Netherlands. All individuals involved in the human post-mortem studies have provided informed written consent for the use of their bodies for scientific research and teaching. All animals were handled in strict accordance with good animal practice as defined in the federal regulations as set forth in the written Assurance of Compliance with PHS Policy to the United States Department of Health and Human Services (Assurance No. A3079-01) and Regulations of the Animal Welfare Act of the United States Department of Agriculture (USDA registration #23-R-0023). All animal work was approved by the Johns Hopkins University Animal Care and Use Committee (ACUC Protocol No. MO15M421) and the animal care program at the Johns Hopkins School of Medicine is fully accredited by the Association for Assessment and Accreditation of Laboratory Animal Care International.

Disclosure of potential conflicts of interest

K.P.F. is an employee of PerkinElmer. All other authors declare no competing financial interests.

Acknowledgments

The authors thank Trishla Sinha and Romano Schreuder for the isolation of staphylococcal strains.

Funding

Part of this research was supported by the Top Institute Pharma projects T4-213 and T4-502 (to J.M.v.D), and by the National Institute of Arthritis and Musculoskeletal and Skin Diseases of the U.S. National Institutes of Health grant

numbers T32 AR067708 (J.M.T. and J.E.P.) and R01AR069502 (L.S.M.). F. Romero Pastrana received a scholarship from CONACyT (169643).

References

1. Tong SYC, Davis JS, Eichenberger E, et al. Staphylococcus aureus Infections: Epidemiology, Pathophysiology, Clinical Manifestations, and Management. *Clin Microbiol Rev.* 2015;28:603–61. doi:10.1128/CMR.00134-14.
2. Peacock SJ, Paterson GK. Mechanisms of Methicillin Resistance in Staphylococcus aureus. *Annu Rev Biochem.* 2015;84:577–601. doi:10.1146/annurev-biochem-060614-034516.
3. Blair JMA, Webber MA, Baylay AJ, et al. Molecular mechanisms of antibiotic resistance. *Nat Rev Microbiol.* 2015;13:42–51.
4. Oosten M van, Hahn M, Crane LMA, et al. Targeted imaging of bacterial infections: advances, hurdles and hopes. *FEMS Microbiol Rev.* 2015;39:892–916.
5. Wang Y, Thompson JM, Ashbaugh AG, et al. Preclinical Evaluation of Photoacoustic Imaging as a Novel Noninvasive Approach to Detect an Orthopaedic Implant Infection. *J Am Acad Orthop Surg.* 2017;25 Suppl 1:S7–12.
6. Ferro-Flores G, Avila-Rodríguez MA, García-Pérez FO. Imaging of bacteria with radiolabeled ubiquickidin by SPECT and PET techniques. *Clin Transl Imaging.* 2016;4:175–82. doi:10.1007/s40336-016-0178-7.
7. Mills B, Bradley M, Dhaliwal K. Optical imaging of bacterial infections. *Clin Transl Imaging.* 2016;4:163–74. doi:10.1007/s40336-016-0180-0.
8. Lazzeri E. Systematic review of in vivo microorganisms imaging with labeled vitamins, bacteriophages and oligomers. *Clin Transl Imaging.* 2016;4:265–272.
9. Rubin RH, Young LS, Hansen WP, et al. Specific and Non-specific Imaging of Localized Fisher Immunotype 1 Pseudomonas aeruginosa Infection with Radiolabeled Monoclonal Antibody. *J Nucl Med.* 1988;29:651–6.
10. Malpani BL, Kadival GV, Samuel AM. Radioimmunoscintigraphic approach for the in vivo detection of tuberculomas—A preliminary study in a rabbit model. *Int J Rad Appl Instrum B.* 1992;19:45–53. doi:10.1016/0883-2897(92)90184-Z.
11. Lee JD, Shin KH, Cho SN, et al. Immunoscintigraphy in the detection of tuberculosis with radiolabelled antibody fragment against Mycobacterium bovis bacillus Calmette-Guérin: a preliminary study in a rabbit model. *Eur J Nucl Med.* 1992;19:1011–5. doi:10.1007/BF00180861.
12. Bardhan NM, Ghosh D, Belcher AM. Carbon nanotubes as in vivo bacterial probes. *Nat Commun.* 2014;5:4918. doi:10.1038/ncomms5918.
13. Oosten M van, Schäfer T, Gazendam JAC, et al. Real-time in vivo imaging of invasive- and biomaterial-associated bacterial infections using fluorescently labelled vancomycin. *Nat Commun.* 2013;4:2584.
14. Dreisbach A, van Dijl JM, Buist G. The cell surface proteome of Staphylococcus aureus. *PROTEOMICS.* 2011;11:3154–68. doi:10.1002/pmic.201000823.
15. Foster TJ, Geoghegan JA, Ganesh VK, et al. Adhesion, invasion and evasion: the many functions of the surface

- proteins of *Staphylococcus aureus*. *Nat Rev Microbiol*. 2014;12:49–62.
16. Olaya-Abril A, Jiménez-Munguía I, Gómez-Gascón L, et al. Surfomics: Shaving live organisms for a fast proteomic identification of surface proteins. *J Proteomics*. 2014;97:164–76. doi:10.1016/j.jprot.2013.03.035.
 17. Lorenz U, Ohlsen K, Karch H, et al. Human antibody response during sepsis against targets expressed by methicillin resistant *Staphylococcus aureus*. *FEMS Immunol Med Microbiol*. 2000;29:145–53. doi:10.1111/j.1574-695X.2000.tb01517.x.
 18. Sakata N, Terakubo S, Mukai T. Subcellular Location of the Soluble Lytic Transglycosylase Homologue in *Staphylococcus aureus*. *Curr Microbiol*. 2005;50:47–51. doi:10.1007/s00284-004-4381-9.
 19. Stapleton MR, Horsburgh MJ, Hayhurst EJ, et al. Characterization of IsaA and SceD, Two Putative Lytic Transglycosylases of *Staphylococcus aureus*. *J Bacteriol*. 2007;189:7316–25. doi:10.1128/JB.00734-07.
 20. Ziebandt A-K, Kusch H, Degner M, et al. Proteomics uncovers extreme heterogeneity in the *Staphylococcus aureus* exoproteome due to genomic plasticity and variant gene regulation. *PROTEOMICS*. 2010;10:1634–44. doi:10.1002/pmic.200900313.
 21. Dreisbach A, Hempel K, Buist G, et al. Profiling the surface of *Staphylococcus aureus*. *PROTEOMICS*. 2010;10:3082–96. doi:10.1002/pmic.201000062.
 22. van den Berg S, Bonarius HPJ, van Kessel KPM, et al. A human monoclonal antibody targeting the conserved staphylococcal antigen IsaA protects mice against *Staphylococcus aureus* bacteremia. *Int J Med Microbiol*. 2015;305:55–64. doi:10.1016/j.ijmm.2014.11.002.
 23. Kong Y, Yao H, Ren H, et al. Imaging tuberculosis with endogenous β -lactamase reporter enzyme fluorescence in live mice. *Proc Natl Acad Sci*. 2010;107:12239–44. doi:10.1073/pnas.1000643107.
 24. Ning X, Lee S, Wang Z, et al. Maltodextrin-based imaging probes detect bacteria in vivo with high sensitivity and specificity. *Nat Mater*. 2011;10:602–7. doi:10.1038/nmat3074.
 25. Panizzi P, Nahrendorf M, Figueiredo J-L, et al. In vivo detection of *Staphylococcus aureus* endocarditis by targeting pathogen-specific prothrombin activation. *Nat Med*. 2011;17:1142–6. doi:10.1038/nm.2423.
 26. Hernandez FJ, Huang L, Olson ME, et al. Noninvasive imaging of *Staphylococcus aureus* infections with a nuclease-activated probe. *Nat Med*. 2014;20:301–6. doi:10.1038/nm.3460.
 27. Bardhan NM, Ghosh D, Belcher AM. M13 Virus based detection of Bacterial Infections in Living Hosts. *J Biophotonics*. 2014;7:617–23. doi:10.1002/jbio.201300010.
 28. Tang EN, Nair A, Baker DW, et al. In Vivo Imaging of Infection Using a Bacteria-Targeting Optical Nanoprobe. *J Biomed Nanotechnol*. 2014;10:856–63. doi:10.1166/jbn.2014.1852.
 29. Miller LS, O'Connell RM, Gutierrez MA, et al. MyD88 Mediates Neutrophil Recruitment Initiated by IL-1R but Not TLR2 Activation in Immunity against *Staphylococcus aureus*. *Immunity*. 2006;24:79–91. doi:10.1016/j.immuni.2005.11.011.
 30. Tsompanidou E, Denham EL, Sibbald MJJB, et al. The Sortase A Substrates FnbpA, FnbpB, ClfA and ClfB Antagonize Colony Spreading of *Staphylococcus aureus*. *PLOS ONE*. 2012;7:e44646. doi:10.1371/journal.pone.0044646.
 31. Schenk S, Laddaga RA. Improved method for electroporation of *Staphylococcus aureus*. *FEMS Microbiol Lett*. 1992;94:133–8. doi:10.1111/j.1574-6968.1992.tb05302.x.
 32. Neef J, Milder FJ, Koedijk DGAM, et al. Versatile vector suite for the extracytoplasmic production and purification of heterologous His-tagged proteins in *Lactococcus lactis*. *Appl Microbiol Biotechnol*. 2015;:1–12.
 33. ter Weele EJ, Terwisscha van Scheltinga AGT, Linssen MD, et al. Development, preclinical safety, formulation, and stability of clinical grade bevacizumab-800CW, a new near infrared fluorescent imaging agent for first in human use. *Eur J Pharm Biopharm*. 2016;104:226–34. doi:10.1016/j.ejpb.2016.05.008.
 34. Cho JS, Guo Y, Ramos RI, et al. Neutrophil-derived IL-1 β Is Sufficient for Abscess Formation in Immunity against *Staphylococcus aureus* in Mice. *PLOS Pathog*. 2012;8:e1003047. doi:10.1371/journal.ppat.1003047.